Evidence for coherent structures within tokamak plasma turbulence

Lifang Dong,* Long Wang, Chunhua Feng, Zanliang Li, Qingxun Zhao,* and Guiding Wang
Institute of Physics, Chinese Academy of Sciences, Beijing 100080, People's Republic of China
(Received 22 September 1997; revised manuscript received 26 January 1998)

Coherent structures of density fluctuations have been observed in the shear region of poloidal rotation of the CT-6B tokamak plasma by analyzing the measured H_α line emission with a wavelet correlation technique. The structures exhibit strong temporal and spatial intermittency with a lifetime of 20–100 μs and a radial size greater than or equal to 1 cm. The fluctuation shows a skewed non-Gaussian probability density function in the region where the coherent structures occur. [S1063-651X(98)09905-X]

PACS number(s): 52.35.Ra, 52.25.Gj, 52.55.Fa

I. INTRODUCTION

Two-dimensional drift wave turbulence models indicate that it is possible for coherent structures to be formed in strongly driven drift wave turbulence [1–4]. The isolated potential fluctuation within a structure is sufficiently large and long lived compared to the diamagnetic drift time scale, the resulting electric field will trap elements of fluids, causing them to move in a coherent fashion along with the fluctuation. Such vortexlike coherent structures have been observed in plasmas in a homogeneous magnetic field [5] or a pure toroidal magnetic field [6,7] and in double-plasma devices [8].

Zweben used a two-dimensional probe array to search for possible coherent structures at the edge of the Caltech tokamak plasma and discovered that the spatial patterns of density fluctuations appear to consist of localized ''blobs'' [9]. However, statistical analysis did not suggest any organized structures associated with the blobs.

Jha *et al.* [10] analyzed the probe data obtained on the ADITYA tokamak and found that the probability density functions (PDFs) of the plasma density and potential fluctuations were non-Gaussian. One possible source of the non-Gaussian behavior in the plasma is coherent structures. However, similar results have not been obtained on the TEXT-U tokamak [11]. Janev *et al.* used a conditional statistical analysis technique to deal with the probe data and have not observed any long-lived coherent structures or obvious non-Gaussian statistics. A biorthogonal decomposition technique has been used to identify coherent structures in the scrape-off-layer turbulence on ADITYA and ASDEX tokamaks [12]. A leptokurtic non-Gaussian statistics has been observed at high frequencies and coherent structures have been observed in the edge plasma on a statistical basis on the ADITYA tokamak [13,14]

The detection of spatial structures of plasma fluctuations is usually conducted on the plane perpendicular to the magnetic field as performed in a homogeneous field or a purely toroidal field using Langmuir probe arrays [5–7]. However, in a tokamak plasma, the correlation measurement simultaneous in poloidal and radial directions is more difficult as the solid probes may disturb the hot plasma.

The spatial resolution measurements of fluctuations in the poloidal direction have been performed in the edge region of a few tokamaks. Since hydrogen atoms form a thin shell structure at the edge of the plasma on medium or large devices, the poloidal structures of plasma turbulence are easy to study through the measurement of the H_α line emission using a focal optical system. The measurement results indicate that the fluctuations show small-scale broadband structures and appear to rotate in the ion diamagnetic direction [15–17]. Magnetic coils were also used to study the poloidal structures of plasma fluctuations and similar results have been obtained [18].

In the TEXT tokamak, a probe setup was used to measure the correlation length in all three directions in the edge region of the plasma [19]. The parallel correlation length was found to be approximately equal to 100 cm and the radial and poloidal correlation lengths are 0.5 and 1 cm, respectively.

In the TFTR tokamak, a beam emission spectroscopy (BES) technique and a method of correlation reflectometry were applied to turbulence measurements [20,21]. The obtained wave-number spectra in the radial and poloidal directions have similar widths, but are seen to be highly anisotropic with respect to the peak in the spectra. The radial spectrum is peaked at $k_r=0$, while the poloidal spectrum shows a peak at $k_\theta \approx 0.5-1.5\ \mathrm{cm}^{-1}$. Hence the turbulence exhibits a wavelet structure in the poloidal direction. The radial and poloidal correlation lengths were 1–2.5 cm in the confinement region. The radial correlation length was found to be 2–4 cm in the main core of the neutral beam heated plasma in the supershot regime.

In this paper we present a radial correlation measurement of plasma fluctuations on the CT-6B tokamak [22]. CT-6B is a small tokamak with a lower plasma temperature. The hydrogen atoms penetrate deeply into the bulk plasma. Such a profile of H_α line emission makes it possible to perform radially resolved measurement of the fluctuation in the outer region of the plasma by monitoring the H_α line emission with a focal optical system. However, since the viewing chords may intersect different radial zones, a measurement of completely localized fluctuations is impossible. A signal obtained with the optical system along a sightline may be attributed to the different radial locations. We have carefully studied the effects on the results of the correlation measurement. In addition, we introduced a correlation technique to

*Present address: Department of Physics, Hebei University, Baoding 071002, People's Republic of China.

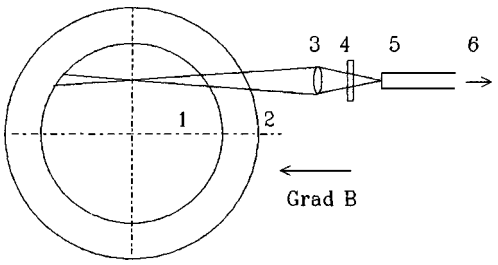

FIG. 1. Experimental setup: 1, plasma; 2, vacuum vessel; 3, lens; 4, filter; 5, optical fibers; 6, photomultiplier tubes.

detect the short-term correlation with intermittent behavior. The results were presented on a two-dimensional time-radius plane and some coherent structures of fluctuations were indicated.

The present paper is organized as follows. In Sec. II the experimental setup and measurement technique are described. In Sec. III the measured plasma parameters are presented. In Sec. IV the correlation analysis and its results are presented. In Sec. V a PDF analysis is presented and its results are compared with that of a correlation analysis. In Sec. VI the experimental results are compared with those of the rotation measurement. Conclusions are given in Sec. VII.

II. EXPERIMENTAL SETUP

CT-6B is a small tokamak with an iron core transformer. The main device parameters are the major radius $R=45$ cm and minor radius of the plasma $a=12$ cm. In the present experiment, the toroidal field $B_t=6$ kG s, the plasma current $I_p=10-15$ kA, the current pulse duration is 50–60 ms, the averaged electron temperature $T_e=150$ eV, the line-averaged electron density $n_e=(1-2)\times10^{13}$ cm^{-3}, and the energy confinement time is 0.5–1 ms. The plasma equilibrium is controlled by a feedback vertical field system.

The standard electromagnetic diagnostics was used to measure the plasma current, loop voltage, and horizontal displacement. The chord-averaged electron density is obtained with a HCN infrared laser interferometer. A radially movable Langmuir probe set on the weak-field side of the equatorial plane monitors the plasma parameters and the fluctuations of the plasma density and potential in the edge region. All radial profiles of plasma parameters in the region were obtained by shot-to-shot discharges.

The imaging optics is shown schematically in Fig. 1. It consists of a simple lens with an aperture of 2.5 cm, a focal length of 5 cm, and an interference filter. The H_α line emission from the viewing chord is imaged onto an eight-channel linear fiber array and monitored with eight photomultiplier tubes.

For the measurement of radial profile of the H_α line emission intensity, the lens–optical-fiber system first views the whole radius of the plasma. After Abel inversion, the chord-integrated emission intensity gives the emissivity of the H_α line as a function of the radius. This measurement ascertains the radial range that is suitable for the fluctuation measurement where the gradient of the emissivity and its fluctuation level on the radius are negative. In this region the central section of a viewing chord contributes dominantly to the signal.

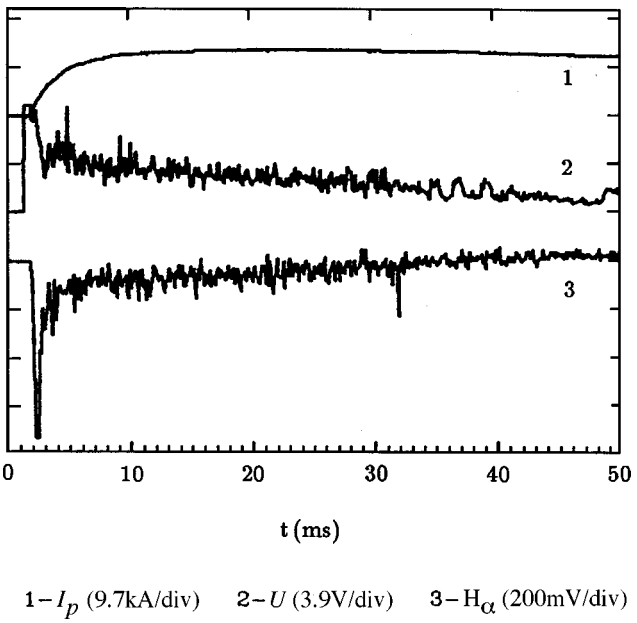

FIG. 2. Set of typical discharge wave forms of 1, plasma current (9.7 kA/div); 2, loop voltage (3.9 V/div); and 3, H_α line emission signal in the seventh channel ($h=8$ cm).

Then the optical system scans in the region of negative gradient, 6–10 cm for the fluctuation measurement. The radial separation between two adjacent channels is 0.57 cm. The measured fluctuation signals were digitized with a sampling time of 3.2 μs.

In the experiment, since the density of hydrogen atoms have a relatively flat profile because of the large mean free path, the plasma density fluctuation can be inferred from the H_α line emission. The intensity of the H_α line emission can be expressed by $n_H n_e \langle \sigma_{ex} v \rangle$. Since the hydrogen atoms have a longer mean free path than the fluctuation scales in the plasmas, their density n_H usually is independent of local plasma parameters. The averaged excitation rate coefficient $\langle \sigma_{ex} v \rangle$ is only weakly dependent on electron temperature in the temperature range of the measurement (20–100 eV). Hence the relative fluctuations of the electron density n_e can be approximately expressed by the relative fluctuations of the H_α line emissivity.

III. MEASUREMENT RESULTS

Figure 2 shows wave forms of the plasma current, loop voltage, and chord-averaged intensity of the H_α line emission in one channel of a typical discharge. All measurements are taken during the plateau phase of the plasma current. The measured integrated intensity of the H_α line emission as a function of height (radial position of the viewing chord) is shown in Fig. 3. The Abel-inverted emissivity is shown in Fig. 4. It peaks between $r=5$ and 6 cm, indicating that the integrated signal measured along a chord with $r\geqslant6$ cm is dominantly contributed by the central part of the chord. Then this radial range is chosen as the region of fluctuation measurement. The relative fluctuation level as a function of the radius is shown in Fig. 5. The absolute fluctuation amplitudes can be obtained approximately by combining the values shown in Figs. 4 and 5.

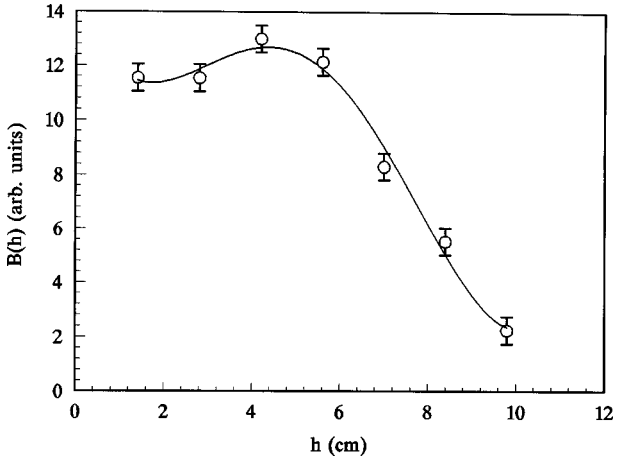

FIG. 3. Chord-integrated intensity of the H_α line emission vs the height of the viewing chord.

We analyze the turbulent fluctuation signals using a fast Fourier transform and a general correlation technique. The power spectrum of the density fluctuation as shown in Fig. 6 exhibits a broadband and follows a power law with an index of approximately 2. The correlation time is 0.1 ms and the correlation length is 0.5–1.3 cm. The results indicate a fully developed turbulent feature of the density fluctuation in the plasma.

A set of typical wave forms of the density fluctuation is shown in Fig. 7. Careful observation of the curves reveals certain short-lived similarities in shape and phase between the signals from adjacent channels, which indicate the existence of intermittent coherent structures of the fluctuations. A quantitative presentation of the structures is obtained by a correlation analysis given below.

IV. CORRELATION ANALYSES

In the measurement geometry, the maximum transverse scale of the image optical cones for each channel is 5 mm. The average transverse scale is comparable to the radial wavelength of the fluctuation. Therefore, the local fluctuation away from the imaged volume on a viewing chord cannot be completely averaged over in the measurement signal. The contributions from the whole viewing chord to the observed

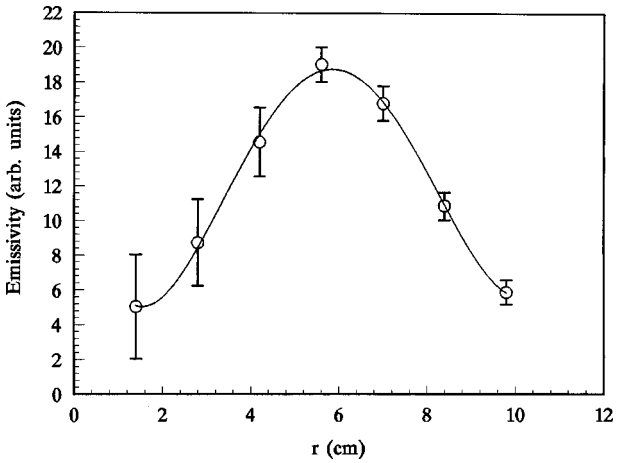

FIG. 4. Emissivity of the H_α line vs the radius of the plasma.

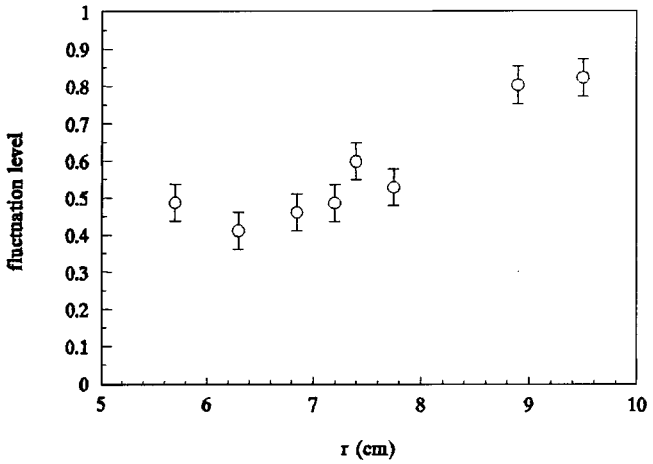

FIG. 5. Relative fluctuation level of the chord-integrated intensity of the H_α line emission vs the height of the chord.

fluctuation should be taken into account. In other words, since a viewing chord intersects different radial zones, the fluctuation measurement on the chord is not completely localized. The measurement signals from different chords may be correlated as they may come from the same radius. We should analyze the effects of the nonlocalization of the measurement geometry on the results of correlation analyses.

Assuming cylindrical symmetry, we partition the cross section of the plasma column into coaxial zones with one zone for each viewing chord as shown in Fig. 8, in which the zones are designated by the subscript j and the viewing chords by the subscript i. The measured signal on the chord i can be written as

$$p_i=\sum_{j=i}^{N}(s_j+s_j')l_{ij}, \tag{1}$$

where s_j and s_j' are, respectively, the local fluctuation amplitudes on the small- and the large-R side in the zone j. l_{ij} is the length matrix

$$l_{ij}=\begin{cases}\sqrt{(r_i+\Delta r/2)^2-r_i^2}, & i=j\\ \sqrt{(r_j+\Delta r/2)^2-r_i^2}-\sqrt{(r_j-\Delta r/2)^2-r_i^2}, & i<j\\ 0, & i>j,\end{cases} \tag{2}$$

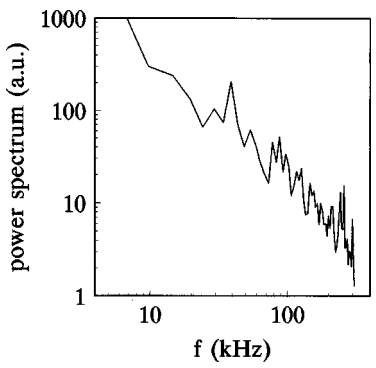

FIG. 6. Power spectrum of the H_α line fluctuation in the seventh channel ($h=8$ cm).

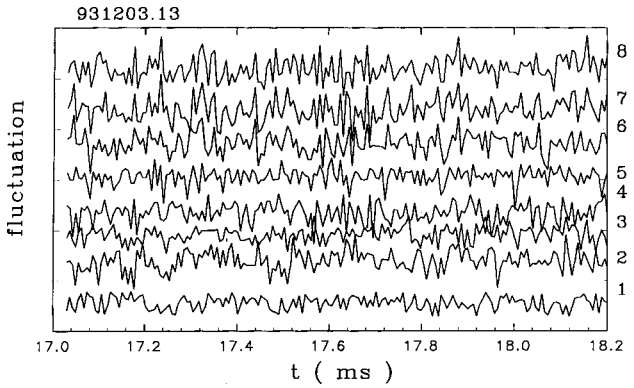

FIG. 7. Typical wave forms of fluctuations in the H_α line emission shown on a short time scale for observation of their correlation. The numbers denote their channels: 1–8 correspond to $r=6-10$ cm.

where Δr is the distance between two adjacent chords, or the zone width. The correlation coefficient without a time delay between the signals from two adjacent viewing chords is

$$c_{i,i-1}=\frac{\langle p_i p_{i-1}\rangle}{\sqrt{\langle p_i^2\rangle\langle p_{i-1}^2\rangle}}, \tag{3}$$

where angular brackets denote a temporally averaged value.

In calculating Eq. (3) we make use of the following assumption. First we suppose that the fluctuation signals from the same side on one zone are completely correlated since they are emitted from the neighboring regions in the same zone

$$\langle s_j s_j\rangle=\langle s_j' s_j'\rangle=\langle s_j^2\rangle. \tag{4}$$

Another finite correlation term is the first cross term $\langle s_i s_i'\rangle l_{ii}^2$ in the calculation of $\langle p_i^2\rangle$. We suppose that they are completely corrected since they are also emitted from the neighboring regions in the same zone. Except for the central section of a chord, the signals from the large-R and small-R sides on the same zone are completely uncorrelated as the distance between the two emission regions is farther than the poloidal correlation length:

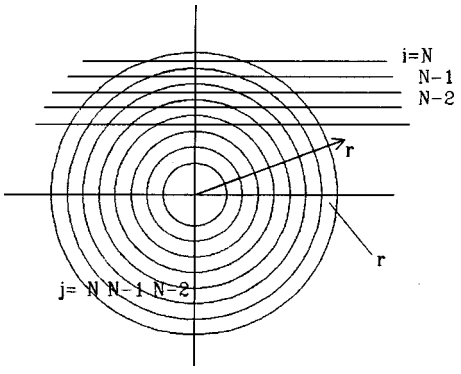

FIG. 8. Measurement geometry.

TABLE I. Fluctuation levels as a function of the radius and the extrapolated values in zones 9 and 10.

i	r (cm)	s
1	6.00	7.20
2	6.57	7.04
3	7.14	6.84
4	7.71	6.57
5	8.29	6.16
6	8.86	5.56
7	9.43	4.76
8	10.00	4.00
9	10.57	3.06
10	11.14	1.80

$$\langle s_j s_j'\rangle=0. \tag{5}$$

Finally, we assume that the fluctuations from the different zones are completely uncorrelated

$$\langle s_j s_k\rangle=\langle s_j' s_k'\rangle=\langle s_j s_k'\rangle=0, \quad j\neq k. \tag{6}$$

Then the correlation coefficient (3) can be obtained from

$$\langle p_i p_{i-1}\rangle=\sum_{j=i}^{N}(\langle s_j^2\rangle+\langle s_j'^2\rangle) l_{ij} l_{i-1,j},$$

$$\langle p_i^2\rangle=4 s_i^2 l_{ii}+\sum_{j=i+1}^{N}(\langle s_j^2\rangle+\langle s_j'^2\rangle) l_{ij}^2. \tag{7}$$

In our experiment, an eight-channel measurement of fluctuations has been performed with the spatial resolution $\Delta r=0.57$ cm in the region $r=6-10$ cm. If we consider the relative fluctuations of signals from the various viewing chords as the relative values of the fluctuation of emissivity at corresponding radii, the fluctuation levels as a function of the radius can be obtained by multiplying the values in Fig. 4 by the corresponding values in Fig. 5 as shown in Table I,

TABLE II. Correlation coefficients between signals from adjacent channels.

Channels $i,i-1$	$c_{i,i-1}$
2,1	0.54
3,2	0.51
4,3	0.48
5,4	0.46
6,5	0.42
7,6	0.39
8,7	0.35

which includes the extrapolated values in zones 9 and 10.

The correlation coefficients between signals from adjacent channels can be obtained from Eqs. (3) and (7) and the above data and are given in Table II.

The above values of the correlation result from the self-correlation of fluctuation signals in the same zones, which, as a background of radial correlation measurements, cannot be eliminated by data processing. Any correlation values exceeding the background indicate a real radial correction.

For presentation of the coherent structures on a time-space plane, combining wavelet [23] and correlation analyses, we suggest a wavelet correlation analysis technique to process the data. We define the wavelet correlation coefficient as

$$\rho(r,t)=\frac{\langle \tilde{I}(r+\Delta r/2,t')\tilde{I}(r-\Delta r/2,t')e^{-(t'-t)^2/2\sigma^2}\rangle}{\sqrt{\langle \tilde{I}^2(r+\Delta r/2,t')e^{-(t'-t)^2/2\sigma^2}\rangle}\sqrt{\langle \tilde{I}^2(r-\Delta r/2,t')e^{-(t'-t)^2/2\sigma^2}\rangle}}, \tag{8}$$

where $\tilde{I}(r\pm\Delta r/2,t)$ are the alternating components of fluctuation signals in the adjacent channels. Their mean values over 100 points have been removed. Expression (8) is different from the conventional correlation coefficient (3) in introducing a wavelet function $e^{-(t'-t)^2/2\sigma^2}$, which is a ''moving window,'' and makes the coefficient a function of time. Its variance σ may be chosen as 12.8 μs, which is less than the self-correlation time. Note that the wavelet correlation coefficient is unity for two signals with complete correlation and with the same phases.

Figure 9 illustrates a contour diagram of the wavelet correlation coefficient in the time-radius plane calculated from the data shown in Fig. 7. Since the self-correlation of the signals originating from the same radial zone due to the nonlocalization of measurement should be taken into account, only the correlation values much higher than the maximum values shown in Table II may be considered as the results of radial correlation. In fact, the values of $\rho(r,t)$ in most of the region, especially for small values of the radius, are much lower than the expected background values caused by the self-correlation shown in Table II. The reason is that the assumption (4) is a very strong condition, which gives an

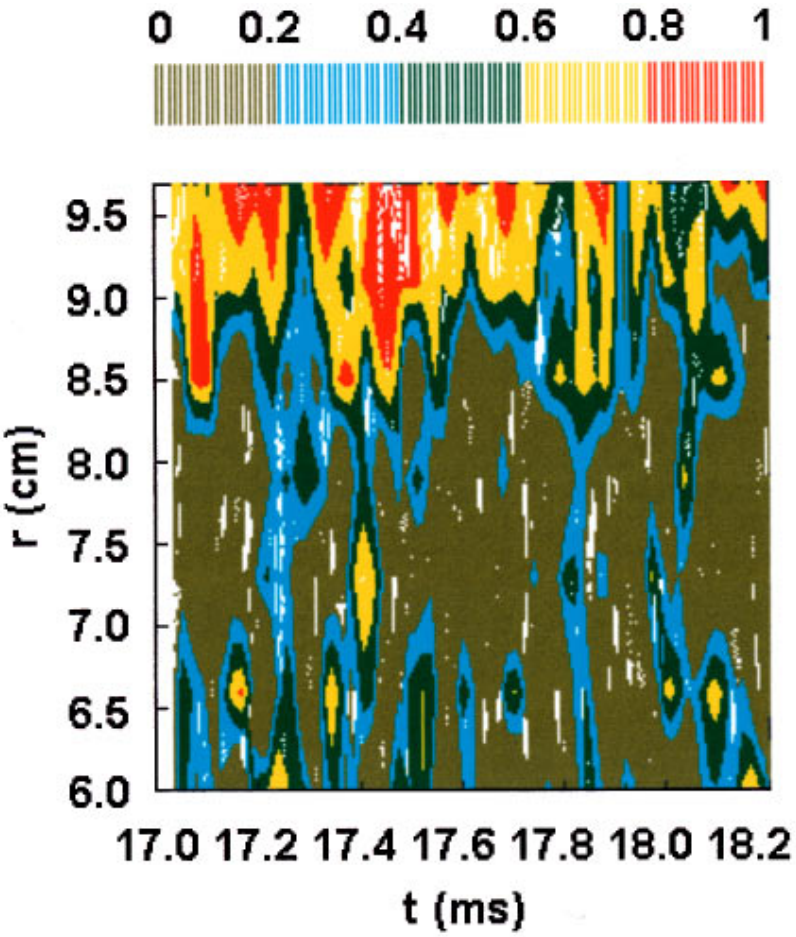

FIG. 9. (Color) Contour diagram of the wavelet correlation coefficient in a time-radius plane obtained from the data shown in Fig. 7.

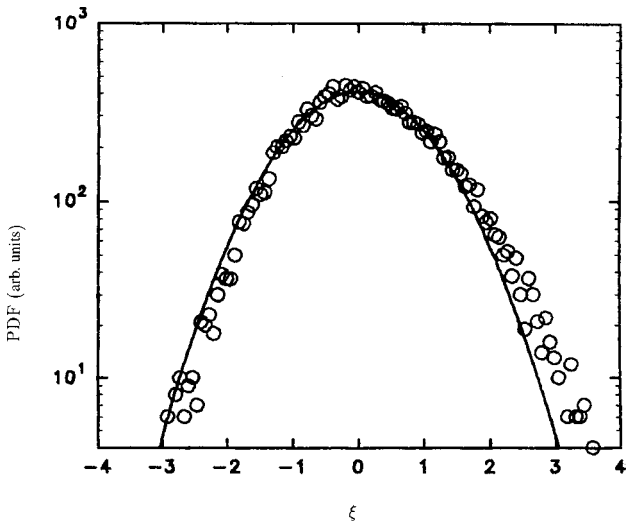

FIG. 10. PDF of the H_α emission line signals in the channel with $r=8$ cm as a function of the fluctuation amplitude and the Gaussian distribution function, shown by the curve. The data were obtained during $t=14-26.5$ ms with a sampling time of 6.4 μs. The relative fluctuation amplitude $\tilde{n}/n$ has been normalized to the variance σ obtained from the fit. $\xi=(\tilde{n}/n)/\sigma$.

upper limit of the background values. Another possible reason is that the small-scale fluctuations away from the imaged volume are partially averaged over.

The diagram in Fig. 9 also shows some irregular, high $\rho(r,t)$ regions, some of which are closed and some open at the boundary of the measured region. The presence of these regions indicates the formation and destruction of some coherent structures in the plasma on a short-time scale. We choose 0.8 as the boundary value of the high $\rho(r,t)$ regions in the diagram and consider the regions (in red) with $\rho(r,t)\geqslant 0.8$ as the domain of coherent structures, since the value is higher than the maximum value of the expected background value in the whole measurement region and much higher than the background values in the edge region. The lifetime of these structures is 20–100 μs and their size in the radial direction is greater than or equal to 1 cm. The larger structure has a longer lifetime. The ratio of the radial width to the lifetime is several 10^2 m/s, which is less than the local diamagnetic drift velocity (several 10^3 m/s, calculated from the local plasma parameters: electron temperature $T_e=20-30$ eV and density scale length $L_n=1-2$ cm). The orientation of the regions is almost perpendicular to the time axis, indicating that the coherent structures do not propagate in the radial direction. The feature is consistent with the measurement result of radial wave-number spectra on the TFTR tokamak [20].

V. PDF ANALYSES

We have also studied the statistical characteristics of density fluctuations in the plasma boundary region by analyzing PDFs of the measured signals of the H_α line emission. As is well known, the PDF becomes Gaussian when modes with completely random phases are superposed. A non-Gaussian PDF may be caused by the presence of intermittency or coherent structures. A PDF obtained from the signals of the

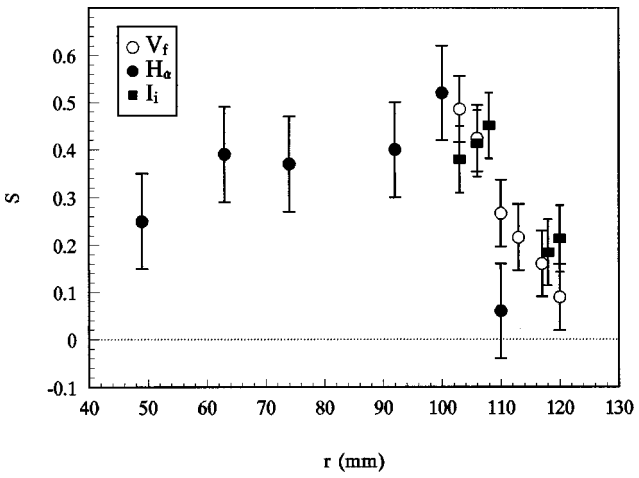

FIG. 11. Skewness of the PDF of density fluctuations vs the radius obtained with the H_α line detection and Langmuir probe and that of the floating potential obtained with the Langmuir probe.

channel with $r=8.5$ cm is plotted in Fig. 10 as a function of fluctuation amplitude, where a Gaussian distribution function fitted with the same variance is also shown by a curve. The distribution function is obviously asymmetric non-Gaussian.

The Gaussian or non-Gaussian properties of a PDF can be quantitatively described by statistical criteria [10]. For a Gaussian PDF its skewness $S=\langle(x-\eta)^3\rangle/\langle(x-\eta)^2\rangle^{3/2}$ is equal to zero and its kurtosis $K=\langle(x-\eta)^4\rangle/\langle(x-\eta)^2\rangle^2$ is equal to 3, where x is a random variable, η is its mean, and $\sqrt{\langle(x-\eta)^2\rangle}$ is the variance. A departure from these values indicates non-Gaussian statistics.

The skewness and kurtosis of the PDF of density fluctuations are calculated from the measured data of the H_α line and plotted as functions of the radius in Figs. 11 and 12, respectively (solid circles). The error bars are taken as the standard deviation of results from shot-to-shot measurements. The results calculated with different sampling times (0.8–6.4 μs) are similar. The skewness shown in Fig. 11 obviously deviates from zero; it is due to the asymmetry of

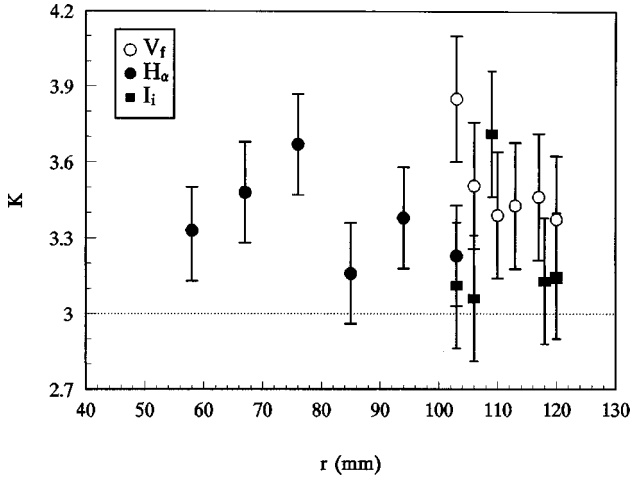

FIG. 12. Kurtosis of the PDF of density fluctuations vs the radius obtained with the H_α line detection and Langmuir probe and that of the floating potential obtained with the Langmuir probe.

the distribution function shown in Fig. 10. It is noteworthy that the departure from Gaussian statistics increases with the radius for $r<10$ cm. The trend is consistent with the distribution of coherent structures in the radius shown in Fig. 9. The kurtosis of the PDF shown in Fig. 12 is higher than 3, but with a high error level. The parameter shows scattering on the radius and is not consistent with the distribution of the observed coherent structures.

A probe measurement of the plasma density and floating potential is also made for comparison. A single Langmuir probe is used to minimize disturbance. The movable probe traverses the radial range of $r=10.2-12$ cm. The fluctuations in the plasma density and the floating potential are analyzed. The obtained values of skewness and kurtosis are also shown in Figs. 11 and 12, respectively (open circles and solid squares). The skewness from the probe measurement agrees with that from the H_α line measurement in the edge region, while the behavior of kurtosis obtained in both methods is similar. Thus both the H_α line and the probe measurement show a skewed non-Gaussian statistics indicating the presence of intermittency or coherent structures in the edge region.

In addition, the theoretical study shows that the coherent structures generated in a two-dimensional drift turbulence may be one of two types: monopole or dipole [3]. They can be experimentally identified by the observed values of skewness and kurtosis. The monopole type has a nonzero skewness and the dipole type produces a kurtosis different from 3. In the present experiment, the observed coherent structures probably are of the monopole type due to the observed departure of skewness values from zero and the correlation of its values with the distribution of coherent structures. The results agree with the theoretical prediction obtained from a numerical simulation [4].

VI. DISCUSSION

Some features of the observed coherent structures such as a long lifetime (compared to the diamagnetic drift time scale), stochastical occurrence in space, dependence of the structure lifetime on their size, and their statistical parameters are consistent with those predicted by the driven drift wave theory and those obtained in some experiments performed in magnetized plasmas. However, the pattern of the structures may possibly be different from that obtained theoretically or experimentally in two-dimensional fluctuations in a homogeneous or a pure toroidal magnetic field due to the existence of magnetic surfaces and the rotation transform in a tokamak configuration. We have not conducted a poloidally resolved measurement of the fluctuation on the device. The results of such measurements conducted on other devices [15–18] show that the fluctuation structures rotate in the poloidal direction. Since the observed structures on the CT-6B tokamak are located near the zero point of the poloidal rotation speed as shown below, the behavior of the coherent structures in the poloidal direction may be different from the results obtained on other devices. Therefore, we cannot determine whether the observed coherent structures are isotropic or anisotropic in the plane perpendicular to the field on the basis of the present experimental data.

In order to determine the location of the observed coherent structures in the plasma, the plasma poloidal rotation measurements based on the spectroscopic Doppler shift have been performed along different viewing chords by using a monochromator-photodiode array detector system. The rotation speed of the impurity ions is in the electron diamagnetic direction in the plasma interior and in the ion diamagnetic direction in the boundary region. An analysis of the results obtained from the measurement for neutral hydrogen atom lines indicates that the main ions rotate in the same poloidal direction as that for impurity ions in the plasma interior. Details of the measurement results will be reported elsewhere. Here only the result for the O II 4642-Å line is given in Fig. 13, which shows the rotation speed of the ions vs the radius. The curve was obtained from the Doppler shift of the spectral line observed along a chord with radius r, but can be regarded as a local quantity except in the central region. The plasma rotates as a rigid body in the interior. The linear speed attains a maximum value of about 2.5 km/s at $r=7$ cm; then it slows down and reverses at $r=10$ cm. The observed coherent structures are located in the shear region of $r=8-12$ cm and near the zero point of the rotation speed if the unmeasured region of $r>10$ cm is ignored. It must be pointed out that the ratio of the radial size of the coherent structures to their lifetime (several 10^2 m/s) is of the same order of magnitude as the poloidal rotation speed in the shear region $r=9-10$ cm. The observed coherent structures and their relations with the poloidal rotation suggest that the coherent structures may be driven by the rotation shear [1]. Their transient property could be interpreted by introducing some dissipation mechanisms.

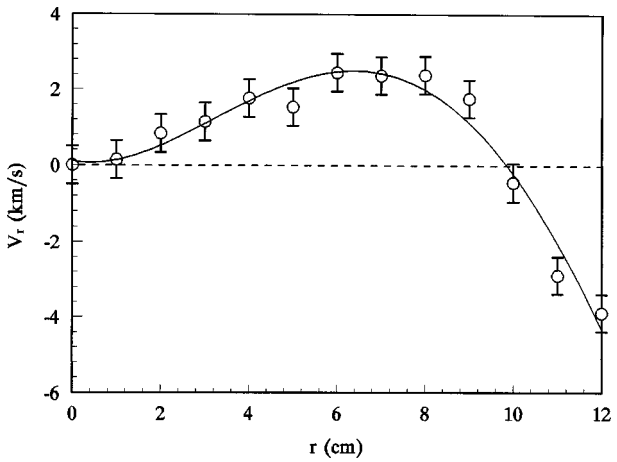

FIG. 13. Poloidal rotation speed of oxygen ions in the first ionized state vs the radius.

VII. CONCLUSIONS

In summary, a wavelet correlation concept has been suggested to treat the fluctuation data. This analytic method is similar to the wavelet bicoherence [24,25] as both are suitable to analyze fluctuation data containing short-lived events. However, the suggested wavelet correlation detects phase coupling between two signals, while the wavelet bicoherence detects that occurring in a single signal. Using the present method to analyze the density fluctuations data with radial resolution, some coherent structures within the plasma turbulence with temporal and spatial intermittency have been di-

rectly presented in the shear region of poloidal rotation of the CT-6B tokamak plasma. Their radial size is greater than or equal to 1 cm and their lifetime is 20–100 μs. The PDF of the fluctuation data is non-Gaussian in the outer region of the plasma, which may be related to the coherent structures and reveals the possible monopole type of coherent structures, though it needs further experimental demonstration.

ACKNOWLEDGMENTS

We would like to thank the CT-6B team for their technical assistance and Professor Jixing Liu for valuable discussions. L.D. and Q.Z. thank the Department of Physics, Hebei University for its support. This work was supported by the National Natural Science Foundation of China and the Chinese Academy of Sciences.

[1] W. Horton and Jixing Liu, Phys. Fluids **27**, 2067 (1984).
[2] A. E. Koniger, J. A. Crotinger, and P. H. Diamond, Phys. Fluids B **4**, 2785 (1992).
[3] J. A. Crotinger and T. H. Dupree, Phys. Fluids B **4**, 2854 (1992).
[4] N. Naulin and K. H. Spatschek, Phys. Rev. E **55**, 5883 (1997).
[5] T. Huld, A. H. Nielson, H. L. Pecseli, and J. J. Rasmussen, Phys. Fluids B **3**, 1609 (1991).
[6] A. K. Singh and Y. C. Saxena, Phys. Plasmas **1**, 2926 (1994).
[7] F. J. Oynes, H. L. Pecseli, and K. Rypdal, Phys. Rev. Lett. **75**, 81 (1995).
[8] H. Johnsen, H. L. Pecseli, and J. Trulsen, Phys. Rev. Lett. **55**, 2297 (1985).
[9] S. J. Zweben, Phys. Fluids **28**, 974 (1985).
[10] R. Jha, P. K. Kaw, S. K. Mattoo, C. V. S. Rao, Y. C. Saxena, and ADITYA Team, Phys. Rev. Lett. **69**, 1375 (1992); G. C. Sethia and D. C. Reddy, *ibid.* **76**, 1003 (1996).
[11] R. K. Janev *et al.*, Nucl. Fusion **29**, 109 (1989).
[12] S. Benkadda, T. Dudok de Wit, A. Verga, A. Sen, ASDEX Team, and X. Garbet, Phys. Rev. Lett. **73**, 3403 (1994).
[13] R. Jha and Y. C. Saxana, Phys. Plasmas **3**, 2979 (1996).
[14] B. K. Joseph, R. Jha, P. K. Kaw, S. K. Mattoo, C. V. S. Rao, Y. C. Saxena, and ADITYA Team, Phys. Plasmas **4**, 4292 (1997).
[15] S. J. Zweben, J. McChesney, and R. W. Gould, Nucl. Fusion **23**, 825 (1983).
[16] P. D. Hurwitz, B. F. Hall, and W. Rowan, Rev. Sci. Instrum. **63**, 4614 (1992).
[17] M. Endler *et al.*, Nucl. Fusion **35**, 1307 (1995).
[18] K. Kiyama and S. Kiyama, Nucl. Fusion **36**, 1113 (1996).
[19] Ch. P. Ritz, H. Lin, T. L. Rhodes, and A. J. Wootten, Phys. Rev. Lett. **65**, 2543 (1990).
[20] R. J. Fonck, G. Cosby, R. D. Durst, S. F. Paul, N. Bretz, S. Scott, E. Synakowski, and G. Taylor, Phys. Rev. Lett. **70**, 3736 (1993).
[21] E. Mazzucato and R. Nazikian, Phys. Rev. Lett. **71**, 1840 (1993).
[22] X. Yang, D. Jiang, W. Li, G. Han, L. Wang, X. Qi, C. Feng, Z. Li, and S. Zheng, Nucl. Fusion **36**, 1669 (1996).
[23] C. Chui, *An Introduction to Wavelet* (Academic, New York, 1992).
[24] B. Ph van Milligan, C. Hidalgo, and E. Sanchez, Phys. Rev. Lett. **74**, 395 (1995).
[25] B. Ph van Milligan *et al.*, Phys. Plasmas **2**, 3017 (1995).